Plasmon-Induced Electrical Conduction in Molecular Devices

Parag Banerjee,[†] David Conklin,[‡] Sanjini Nanayakkara,[‡] Tae-Hong Park,[§] Michael J. Therien,[⊥] and Dawn A. Bonnell[‡,*]

[†]Department of Materials Science and Engineering, University of Maryland, College Park, Maryland, 20742, [‡]Department of Materials Science and Engineering, University of Pennsylvania, Philadelphia, Pennsylvania, 19104, [§]Department of Chemistry, University of Pennsylvania, Philadelphia, Pennsylvania, 19104, and [⊥]Department of Chemistry, Duke University, Durham, North Carolina, 27708

ABSTRACT Metal nanoparticles (NPs) respond to electromagnetic waves by creating surface plasmons (SPs), which are localized, collective oscillations of conduction electrons on the NP surface. When interparticle distances are small, SPs generated in neighboring NPs can couple to one another, creating intense fields. The coupled particles can then act as optical antennae capturing and refocusing light between them. Furthermore, a molecule linking such NPs can be affected by these interactions as well. Here, we show that by using an appropriate, highly conjugated multiporphyrin chromophoric wire to couple gold NP arrays, plasmons can be used to control electrical properties. In particular, we demonstrate that the magnitude of the observed photoconductivity of covalently interconnected plasmon-coupled NPs can be tuned independently of the optical characteristics of the molecule—a result that has significant implications for future nanoscale optoelectronic devices.

KEYWORDS: gold nanoparticles · porphyrin · surface plasmons · photoconduction

Plasmonics and molecular electronics are two fields that explicitly exploit nanoscale physical phenomena. In plasmonics, optical interactions with nanosized particles induce SPs creating locally intense electromagnetic fields. Plasmons have been shown to direct light transmission[1,2] and increase sensitivity in molecular spectroscopy to enable targeted tumor treatment[3] as well as molecular recognition labeling.[4] Recently, SPs have been used to affect the optical properties of organic molecules, enabling exciting new strategies for optical circuits.[5] Research in molecular electronics has also intensified in the last two decades and has focused on electrical conduction in organic molecules to enable useful devices.[6−9] The effects of molecular length, conjugation, and electrode work function on properties have been quantified. The critical nature of molecule−electrode connectivity has been interrogated theoretically and experimentally.[10,11]

In spite of the rapid progress in these two fields, interaction of optically induced plasmons with charge migrating through single molecules has not been observed to date. Here, we demonstrate the ability of a plasmon to alter the electrical properties of a molecular junction. To successfully observe this phenomenon, two fundamentally critical and deliberate choices in preparing devices were made. First, the device platform consists of an array of Au NPs fabricated on insulating glass substrates. Disordered metallic NP arrays like the one shown within the device in Figure 1a have been extensively studied in the past due to their interesting plasmonic properties and as models of transport in granular materials.[12,13] Consequently, these arrays form an ideal platform on which to study plasmon interactions and their impact on molecular conduction. Electronic transport in these systems depends upon the distribution of and separation between the NPs. Whereas NP sizes can be controlled *via* modification of synthetic conditions, interparticle distances are usually determined by the nature of the conjugated molecular species that link the NPs. High density, close packed NP arrays exhibit metallic conductivities with resistances higher than that of the bulk material due to electron scattering at NP boundaries. At larger interparticle separations, electrons can tunnel between NPs; for such systems, temperature-dependent transport data may exhibit an Arrhenius dependence ($\sigma \propto \exp T^{-1}$) or suggest other conduction mechanisms (e.g., $\sigma \propto \exp T^{-1/2}$).[14] In all cases however, conduction occurs *via* a percolative path spanning from one electrode to another that comprises the "path of least resistance".[15] One of the critical goals in these experiments was to produce arrays in which the average separation between neighboring NPs corresponded to the length scale of a rigid, highly conjugated molecule that featured appropriate linkage

*Address correspondence to bonnell@lrsm.upenn.edu.

Received for review September 3, 2009 and accepted January 13, 2010.

Published online January 22, 2010.
10.1021/nn901148m

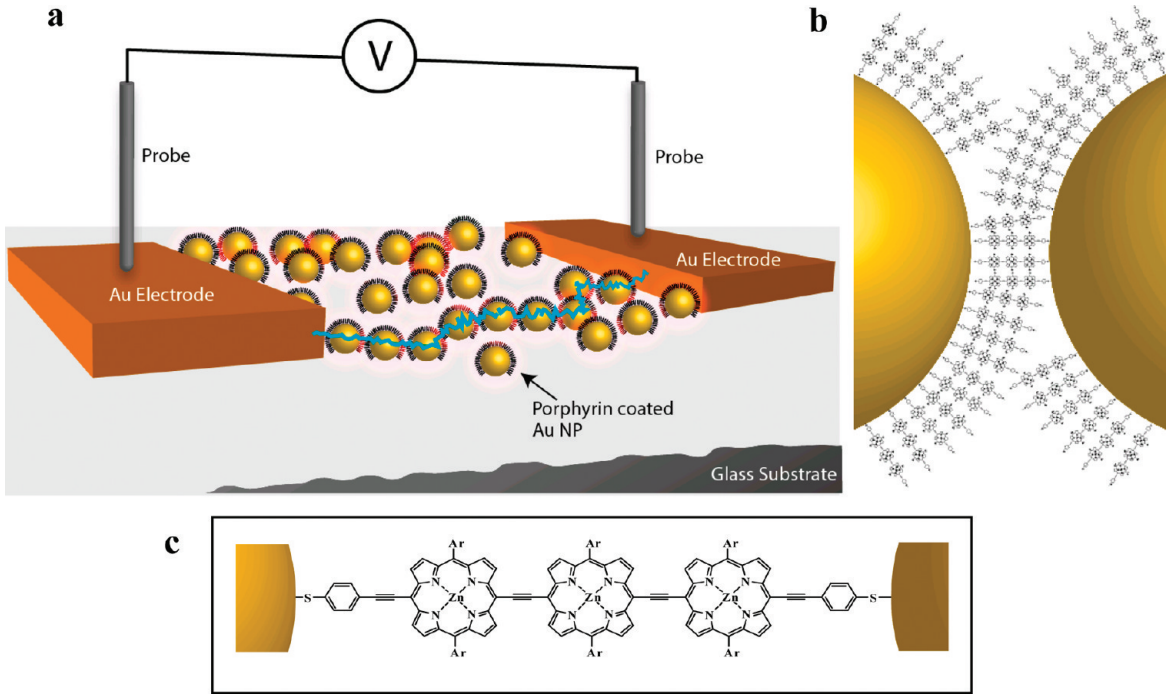

Figure 1. Schematic representation of the hybrid molecular device. (a) The hybrid device used to measure plasmon-mediated photoconductance in the multichromophoric molecule, dithiol−PZn_3−AuNP percolation pathway, with interparticle distances on the order of the length of the molecular S-to-S distance (~4.6 nm). (b) Individual AuNPs that are ~5 nm apart may incorporate more than one dithiol−PZn_3 interconnect. AuNPs were coated with dithiol−PZn_3 molecules through a ligand displacement reaction involving citrate-stabilized AuNPs. (c) The chemical structure of AuNP bound dithiol−PZn_3.

functionality at its termini to ensure a percolative conduction path in the device. Such a AuNP−AuNP interconnect is shown schematically in Figure 1b.

The second choice was to select molecular interconnects that are not only well matched to NP physical properties, but possess optoelectronic characteristics optimal for coupling to Au SPs. For example, since isolated and coupled plasmon resonances in the AuNP systems occur at wavelengths ≥520 nm, a large absorptive oscillator strength in this regime of the electromagnetic spectrum constitutes a critical molecular characteristic for the AuNP−AuNP interconnect. *Meso*-to-*meso* ethyne-bridged (porphinato)zinc(II) oligomers (PZn_n compounds) manifest this spectroscopic property.[16] Moreover, these structures feature intense low-energy, high-oscillator-strength $\pi-\pi^*$ absorptions polarized exclusively along the long molecular axis, and have been established to provide substantial polaron delocalization lengths, impressive dark conductivities, and unusually large polarizabilities.[17−19] These molecular properties can thus play crucial roles in coupling to plasmon resonances and enhancing electro-optic performance of nanoscale devices. Figure 1c shows the structure of an α,ω-dithiol-terminated *meso*-ethyne-bridged porphyrin supermolecule (dithiol−PZn_3), which serves as a 4.6 nm long AuNP-to-AuNP bridge in these devices.

RESULTS

First, the conductivity of the device was characterized in the absence of particles and molecules to quantify possible substrate surface conduction and provide a baseline for the zero conduction case (Supporting Information, Figure S1). Next, the conductivity of the nanoparticle arrays was evaluated. This was found to be a strong function of nominal particle size, density, and minimum particle separation. As an illustration, Figure 2 panels a, b, and c compare the morphologies of 16, 32, and 46 nm AuNPs; the areal coverage of the par-

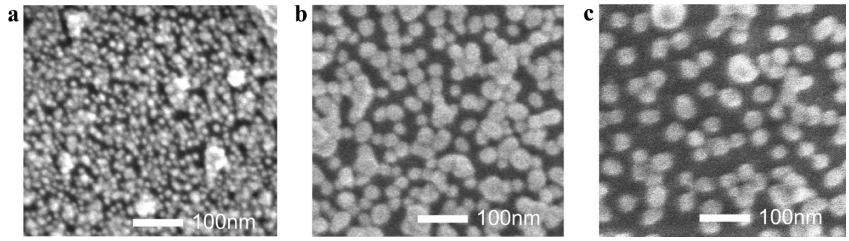

Figure 2. SEM images of AuNP assemblies on glass substrates: (a) 16 nm AuNPs with 52 ± 3% area coverage, (b) 32 nm AuNPs with 54 ± 3% area coverage, and (c) 46 nm AuNPs with 46 ± 2% particle area coverage.

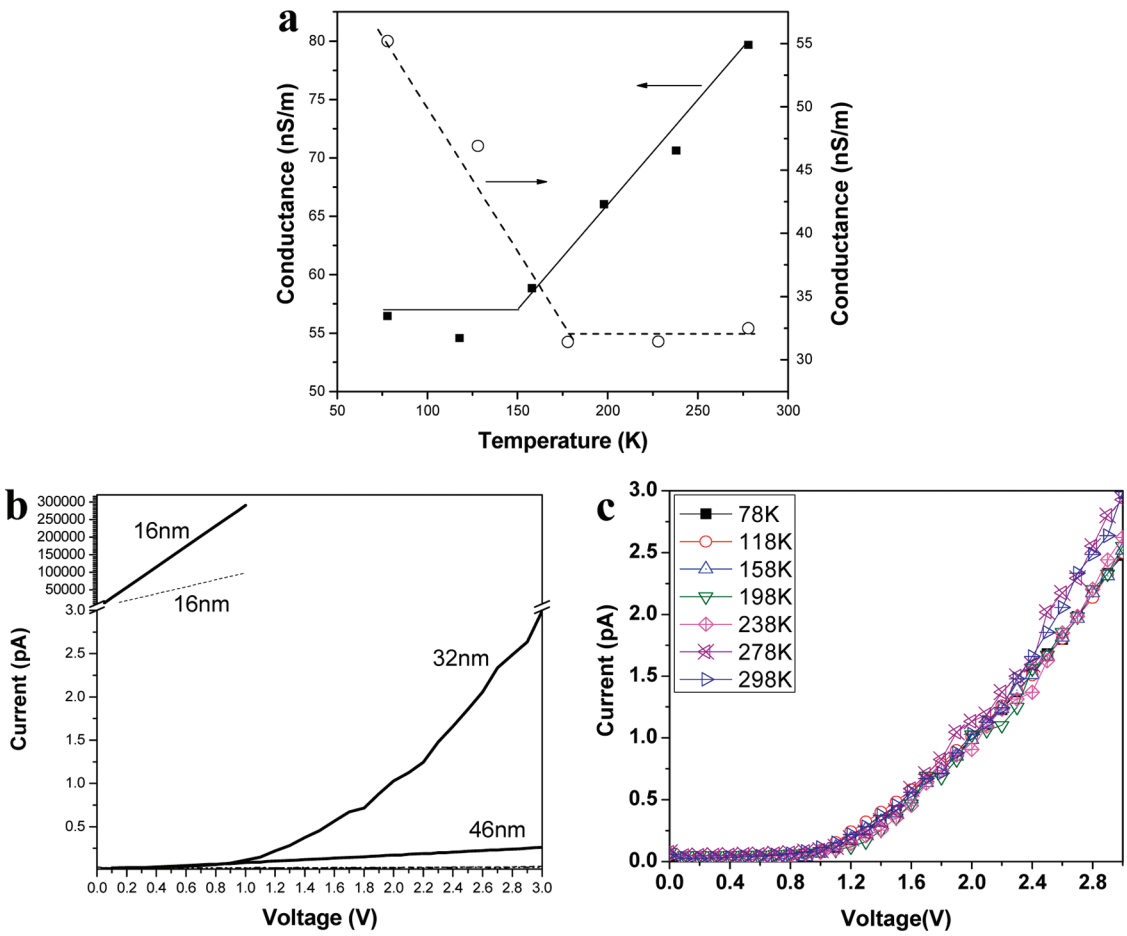

Figure 3. IV characteristics of AuNP assemblies: (a) The temperature dependent conductivity of 16 nm AuNP assemblies, exhibiting metallic (dotted) or semiconducting (solid) behavior as a function of NP surface coverage. (b) Room temperature *I*−*V* characteristics of 16, 32, and 46 nm AuNP-based devices with (bold) and without (dashed) dithiol−PZn_3 interconnects. The *I*−*V* behavior of 32 and 46 nm AuNPs without adsorbed dithiol−PZn_3 lies in the noise level of the system. (c) Typical *I*−*V* curves obtained for a device based on 32 nm AuNPs and dithiol−PZn_3 molecules as a function of temperature. Corresponding Arrhenius plots are provided in Supporting Information, S6.

ticles in these devices were 52 ± 3%, 54 ± 3%, and 46 ± 2%, respectively. Figure 3a illustrates conductance of two high density 16 nm arrays. In one, the conduction decreases with increasing temperature as expected for a metallic array (dotted), while in another, conductivity increases with increasing temperature (solid) showing a thermally activated conduction process. These samples demonstrate the metal−insulator transition that occurs at a critical particle density.[14] Note that while this conductivity is 7 orders of magnitude higher than that of any substrate leakage, it is much lower than that for metal films, indicating that only a fraction of the particles provide conducting pathways. These results demonstrate the versatility of disordered AuNP arrays in providing a test platform with a diverse set of device morphology and characteristics.

After dithiol−PZn_3 adsorption, all samples irrespective of the AuNP size exhibited enhanced conductivity as shown in Figure 3b. Notice that the 32 nm AuNP IV characteristics shift from near negligible to a threshold-based IV after dithiol−PZn_3 attachment—an indication that a large fraction of dithiol−PZn_3-linked AuNPs are now participating in the conduction process.[20] Such threshold-based conduction mechanisms are characteristic of molecularly linked disordered metal nanoparticle arrays where conduction occurs *via* a percolative pathway.[21] The effect of temperature on transport in 16, 32, and 46 nm AuNP systems that feature adsorbed dithiol−PZn_3 was also evaluated, and is shown in Figure 3c for the 32 nm sample. This temperature-dependence study allows extraction of activation energies (E_a). E_a values of 3 and 6 meV were obtained over a $158 < T < 298$ K temperature domain for dithiol−PZn_3-bound 16 and 32 nm-sized AuNPs, respectively. Similar E_a values have been reported previously for metallic nanoparticle disordered arrays separated by linker molecules.[14,22]

The 46 nm AuNP-based device shows negligible change in conductivity as a function of temperature. Apparently, the density of particles (areal coverage ~46 ± 2%) is below the critical point for percolation and the distance between particles in these arrays is sufficiently large to preclude tunneling between the particles and molecular linking. This sample was therefore

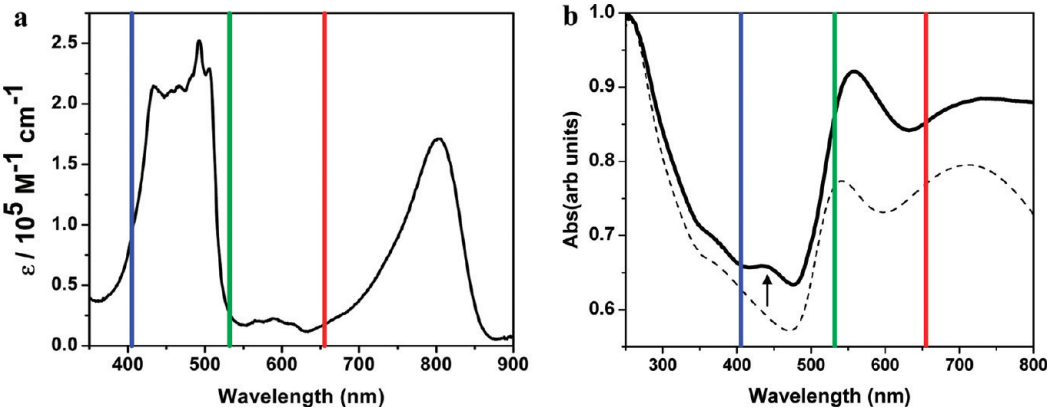

Figure 4. Optical properties of the dithiol−PZn_3 molecule and AuNP linked dithiol−PZn_3 assemblies. (a) Absorption spectrum of dithiol−PZn_3 in tetrahydrofuran solution. The blue, green, and red lines overlaid on the absorption spectrum indicate the incident laser irradiation wavelengths. (b) Absorption spectrum of AuNPs on glass (dash) and AuNPs that feature surface adsorbed dithiol−PZn_3 (solid) molecules (note the absorption at ~ 450 nm, highlighted by the arrow). Note also that the AuNP absorption bands slightly red shift after dithiol−PZn_3 attachment due to the reduction in the effective medium dielectric constant.

not used to study the potential impact of electromagnetic fields generated by SPs on neighboring NPs upon dithiol−PZn_3 attachment. In contrast, as shown above, a series of 32 nm-sized AuNP arrays which are insulating in the absence of adsorbed dithiol−PZn_3, but change dramatically upon AuNP functionalization were chosen to probe the extent to which plasmon-molecule interactions modulate photoconductivity.

Remarkable differences are observed in the photocurrent responses as a function of excitation wavelength. Illumination with 655 (red), 532 (green), and 405 nm (blue) wavelength light causes an increase in the conductivity over that of the dark current. Since neither conductivity nor photoresponse manifests in these arrays in the absence of dithiol−PZn_3, the photocurrent must derive from optical interactions with the molecule. If the magnitude of the photocurrent depended only upon production of the electronically excited singlet state of the AuNP-to-AuNP linker, the measured photoconductivity should track with the magnitude of the wavelength-dependent absorptive extinction coefficient. Figures 4a and 4b compare the absorbance of dithiol−PZn_3 in solution[19] and attached to AuNPs, respectively. As it is known that a thiol-to-Au connectivity does not substantially alter the electronic structure of a wide range of adsorbed molecules,[10] molecular photoconductivity should be proportional to the absorption at the relevant wavelength in Figure 4a, that is, low on illumination with red and green light and 3−4 times higher for blue light. This is clearly not the case as illustrated in Figure 5a which shows the $I-V$ curves of a single device under various illumination conditions and Figure 5b which shows the increase in current $\triangle I_{red}$, $\triangle I_{green}$, and $\triangle I_{blue}$ over the dark current at 1 V, normalized for laser power.[23] $\triangle I_{red}$ is 2−12 times higher than $\triangle I_{green}$ or $\triangle I_{blue}$ at various voltages and over a broad 78−278 K temperature range.

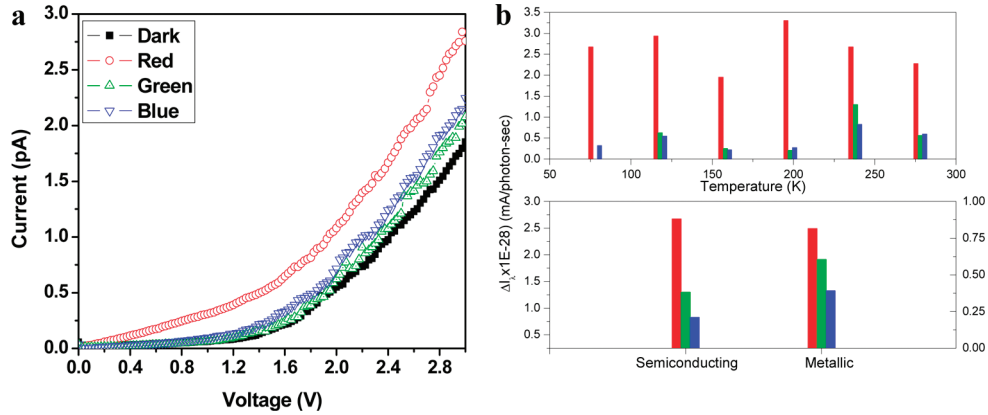

Figure 5. $I-V$ characteristics under optical excitation in AuNP linked dithiol−PZn_3 assemblies. (a) Laser irradiation wavelength dependent $I-V$ characteristics of the 32 nm AuNP devices with dithiol−PZn_3 interconnect. (b) Increase in current over the dark current $\triangle I_\lambda$ at 1 V, per incident photon per second, of the AuNP-based devices that feature surface adsorbed dithiol−PZn_3 molecules. The colored histogram bars represent the laser used—red for 655 nm, green for 532 nm, and blue for 405 nm. The upper plot shows the temperature dependence of $\triangle I_\lambda$ of the semiconducting sample, while the lower plot compares semiconducting and metallic samples at 230 K. Both samples show that the greatest increase in current is observed while exposing the samples to red laser illumination.

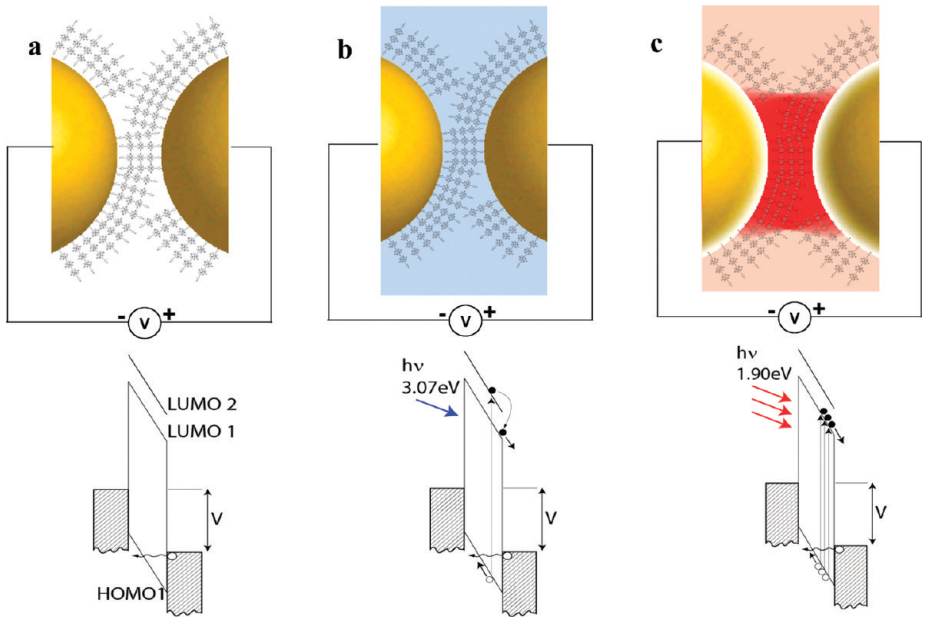

Figure 6. Schematic representations of AuNP coupling with dithiol−PZn_3 molecules and corresponding energy level diagrams: (a) in dark, an applied voltage results in hole tunneling through the small barrier; (b) in the presence of blue light, an initially prepared exciton state relaxes to a lower energy state, producing excess current; (c) in the presence of red light, coupled resonating SPs focus excitation between particles leading to multiple exciton states and higher current.

DISCUSSION

To understand the anomalously large photocurrent observed for 655 nm illumination, it is important to consider the possible effect of SPs. The optical absorption due to plasmons in gold nanoparticles depends on particle size and the coupling between particles. Figure 4b highlights the optical absorption for arrays functionalized with dithiol−PZn_3. The primary plasmon peak near 550 nm and the particle coupling absorption centered at 700 nm both broaden and shift to longer wavelength as particle size increases, as expected: the dithiol−PZn_3 transition at 450 nm is unaffected by AuNP size variation. For these arrays a contribution to the conduction from a plasmon-induced interaction could thus occur for illumination with red and green light, but not with blue light.

To further illustrate the plasmon interaction, a parameter *E*, the enhancement factor, is introduced, that quantifies the plasmon enhanced electrical conduction where, $E = \Delta I_\lambda / \Delta I_{blue}$ and $\triangle I_\lambda$ is the increase in current as defined above[23] at wavelength λ (where λ = red, green, or blue). As an illustration, for the case of the 32 nm AuNP-based semiconducting device at 1 V and 278 K, $E = 1$ for blue light since no plasmon effect can contribute to the current based on the argument in the previous paragraph. Thus, an enhancement factor of 1 corresponds to conventional photocurrent, where conventional photocurrent is that occurring in the absence of any plasmon fields. A large E therefore quantifies the effect of plasmon interaction. The conventional photocurrent should therefore be directly proportional to the absorption oscillator strength at 405 nm in Figure 4a. The photocurrent for red and green illumination should be smaller by a factor of ∼4 to 8 since the absorption at those wavelengths is much less intense. Instead, Figure 5b shows that the green light induced current is about the same and the red light induced current is much larger than that induced by the blue light. Over various samples and temperatures, *E* varied from 0.8 to 1.6 for green light and from 2.1 to 12.1 for red light. Such enhancement factors are much higher than those reported recently in alkane-linked AuNP arrays which show a bolometric enhancement of current conduction that derives from surface plasmon excitation.[24] If Arrhenius based, thermally activated processes are responsible for the increased conductance, then based on the 5 meV E_a, an unrealistically high temperature of ∼1875 K would be required to account for the observed enhanced conductivity. Thus, these enhancements cannot be related to purely thermal effects.

The energies of relevance to transport, the highest occupied (HOMO) and lowest unoccupied (LUMO) molecular orbital are illustrated in Figure 6. The Fermi level of the nanoparticles is 0.415 eV below the middle of the HOMO−LUMO gap of dithiol−PZn_3.[25] The sulfur−gold bond at the interface plays a significant role in fixing this barrier to transport, and although some electron localization at this interface is inevitable, for the purpose of our discussion we assume that the barrier height does not change appreciably. The PZn_3 π-system within the linker is however completely delocalized and presents a near barrierless path for charge transport.[19] This is consistent with the computed dithiol−PZn_3 conductance at a given AuNP−AuNP junction (∼0.12 nS; Supporting Information, S7) and ex-

perimental data obtained for closely related systems.[26] Upon application of a bias, hole mediated tunneling occurs as shown in Figure 6a. Following the analysis of Beebe[27] our data indicate that the dark current transition from tunneling to Fowler−Nordheim transport occurs at 1.0 V (see Supporting Information Figure S2). Illumination with blue light results in conventional photoconductivity as shown in Figure 6b. Optical absorption creates an exciton and the positive and negative charge carriers are separated in the electric field, contributing to the current. Absorption at 3.07 eV produces hole and electron carriers; this initially prepared state relaxes to a lower energy exciton state within femtoseconds where it contributes to the current.[28] The current increase is correlated with the number of carriers and consequently to the photon flux, absorption efficiency, and excited state lifetimes.

In the case where the optical radiation excites a SP and the nanoparticles are optimally coupled, a large electromagnetic field is established between the particles. In the configuration shown in Figure 6c, the particles act as optical antennae and focus light into the small region between the particles.[29] The size, shape and separation can be tailored to engineer the region of focused light. This focusing effect has the consequence of increasing the photon flux at the molecular junction. When the size, shape and separation of the particles are optimized to produce a "resonant" optical antennae, enhancement factors as high as 10^4 result.[30] The results summarized in Figure 6 illustrate how this effect can be used to transduce light into electrical conduction. To generalize this process, the nanoparticle array can be engineered to sharpen or shift the plasmon and coupling energies, as well as the antennae enhancement factor, while the molecule can be designed to control the absorption wavelength, oscillator strength, and the nature of exciton and polaron states.

CONCLUSIONS

These results have demonstrated the transduction of optical radiation to current in a molecular circuit. The optical radiation is first captured by AuNPs resulting in SPs. By utilizing a random, network array of AuNPs, SPs of neighboring AuNPs can be coupled to one another forming a percolative path across opposing electrodes. As demonstrated above, the size and separation of the AuNPs can be easily used to tune the coupling of SPs and the resulting plasmonic properties. The optical focusing that can result from this plasmon coupling has been exploited to control electronic properties of molecular circuits. In this work, molecular interconnects that demonstrate large oscillator strength in the same electromagnetic regime as the coupled SPs have been used to successfully demonstrate the optical transduction effect in single molecules. Enhancement factors as high as 12.1 for red light over blue have been shown to exist in spite of a lower photon absorption cross section of the molecule in the red region. This enhancement has been attributed to the optical focusing and increased photon flux resulting from coupled SPs in AuNP network arrays. Since molecular compounds exhibit a wide range of optical and electrical properties, the strategies for fabrication, testing and analysis elucidated in this paper can form the basis of a new set of devices in which plasmon controlled electrical properties of single molecules could be designed with wide implications to plasmonic circuits and optoelectronic and energy harvesting devices.

MATERIALS AND METHODS

To fabricate nanoparticle arrays, glass substrates (Fisher) were cleaned in piranha solution (1:3 30% H_2O_2: concentrated H_2SO_4) for 10 min, rinsed with ultrapure water, and immediately immersed into a 5% solution of 3-aminopropyl-methyl-diethoxysilane (Sigma-Aldrich) in hexane (HPLC grade, Sigma-Aldrich). The glass substrates were kept in this solution at 80 °C for 24−48 h. Citrate-stabilized AuNPs of diameters 16, 32, and 46 nm were synthesized according to a previously published methodology.[31] The amine-functionalized glass substrates were then immersed in aqueous solutions of AuNPs for ~96 h under ambient conditions. It was found that this dip time provided essentially saturated particle densities; sample-to-sample variations in measured particle densities was ~10%. The surface coverage and the particle size distribution of the AuNPs were established using dynamic light scattering (DLS) and scanning electron microscopy (SEM) in the as-prepared colloid, and on the substrate, respectively. Both techniques independently confirmed the size and size distribution of AuNPs.

Processing sequence for dithiol−PZn_3 is provided in Supporting Information, S3. Adsorption of dithiol−PZn_3 onto the AuNP arrays was performed under a nitrogen (ultrahigh purity grade) atmosphere in a glovebox (PlasLabs). The solvent tetrahydrofuran (THF, HPLC grade, Fisher) was distilled from sodium under nitrogen and collected into a vacuum-sealed flask (Chemglass) and subjected to repeated freeze−pump−thaw−degas cycles. For these studies, the THF solvent was subject to multiple (up to eight) freeze−pump−thaw−degas cycles as this step was found to be critical in promoting successful dithiol−PZn_3 attachment to the AuNPs. To an acetyl-protected dithiol−PZn_3 solution (~1 μM in THF), 4 μL/mL of NH_4OH was added to unmask the thiolate functionality. The glass substrates with surface-bound AuNPs were then immersed into adsorption vials (Wheaton) containing this solution and set aside for 4 h. The substrates were rinsed with THF and dried under a stream of N_2. Molecular attachment to the AuNPs was verified *via* electronic absorption spectroscopy, which showed the characteristic chromophore transition centered at 450 nm, and the AuNP plasmon band.[32] Furthermore, the Raman spectra of these samples showed the strong surface-enhanced, characteristic peaks associated with the linker porphyrin system (see Supporting Information Figure S4).[33,34] Gold electrodes (~35 nm thick) separated by thin channels were thermally evaporated (Thermionics) on the AuNP covered glass substrate using a shadow mask technique. Channel lengths between the electrodes varying from 18 to 68 μm were obtained with this technique. The photoresponse of the devices described in this paper was found to be independent of this channel length. The samples were then transferred immediately to the probe station for electrical measurements. At least three samples (four devices/sample) per AuNP size were electrically probed. The transport measurements were obtained using a Lakeshore Desert Cyrogenics TT6 probe station under

vacuum and cooled using liquid nitrogen. Current−voltage ($I-V$) characteristics were acquired with an electrometer (Keithley 6515A) using CuBe probe tips. After obtaining the transport data in the absence of illumination, the wavelength dependent current−voltage characteristics were obtained by exposing the samples to 405 nm (5 mW), 532 nm (2 mW), and 655 nm (5 mW) laser diodes (Edmund Optics). Transport properties were determined at temperatures ranging from 78−298 K.

Acknowledgment. This work was supported by the Nano/Bio Interface Center; National Science Foundation NSEC DMR-0425780. P.B. acknowledges the financial support of the John and Maureen Hendricks Energy Fellowship. M.J.T. acknowledges partial support from the Department of Energy.

Supporting Information Available: Supplementary figures; processing scheme for dithiol−PZn_3; calculations. This material is available free of charge *via* the Internet at http://pubs.acs.org.

REFERENCES AND NOTES

1. Maier, S. A.; Atwater, H. A. Plasmonics: Localization and Guiding of Electromagnetic Energy in Metal/Dielectric Structures. *J. Appl. Phys.* **2005**, *98*, 011101(1)−011101(10).
2. Barnes, W. L.; Dereux, A.; Ebbesen, T. W. Surface Plasmon Subwavelength Optics. *Nature* **2003**, *424*, 824–830.
3. Loo, C.; Lowery, A.; Halas, N.; West, J.; Drezek, R. Immunotargeted Nanoshells for Integrated Cancer Imaging and Therapy. *Nano Lett.* **2005**, *5*, 709–711.
4. Taton, T. A.; Mirkin, C. A.; Letsinger, R. L. Scanometric DNA Array Detection with Nanoparticle Probes. *Science* **2000**, *289*, 1757–1760.
5. Pala, R. A.; Shimizu, K. T.; Melosh, N. A.; Brongersma, M. L. A Nonvolatile Plasmonic Switch Employing Photochromic Molecules. *Nano Lett.* **2008**, *8*, 1506–1510.
6. James, D. K.; Tour, J. M. Electrical Measurements in Molecular Electronics. *Chem. Mater.* **2004**, *16*, 4423–4435.
7. Yu, H. B.; Luo, Y.; Beverly, K.; Stoddart, J. F.; Tseng, H. R.; Heath, J. R. The Molecule−Electrode Interface in Single-Molecule Transistors. *Angew. Chem., Int. Ed.* **2003**, *42*, 5706–5711.
8. Nitzan, A.; Ratner, M. A. Electron Transport in Molecular Wire Junctions. *Science* **2003**, *300*, 1384–1389.
9. Green, J. E.; Choi, J. W.; Boukai, A.; Bunimovich, Y.; Johnston-Halperin, E.; Delonno, E.; Luo, Y.; Sheriff, B. A.; Xu, K.; Shin, Y. S. A 160-Kilobit Molecular Electronic Memory Patterned at 10^{11} Bits per Square Centimetre. *Nature* **2007**, *445*, 414–417.
10. Xue, Y. Q.; Datta, S.; Ratner, M. A. Charge Transfer and "Band Lineup" in Molecular Electronic Devices: A Chemical and Numerical Interpretation. *J. Chem. Phys.* **2001**, *115*, 4292–4299.
11. Nikiforov, M. P.; Zerweck, U.; Milde, P.; Loppacher, C.; Park, T. H.; Uyeda, H. T.; Therien, M. J.; Eng, L.; Bonnell, D. The Effect of Molecular Orientation on the Potential of Porphyrin−Metal Contacts. *Nano Lett.* **2008**, *8*, 110–113.
12. Ghosh, S. K.; Pal, T. Interparticle Coupling Effect on the Surface Plasmon Resonance of Gold Nanoparticles: From Theory to Applications. *Chem. Rev.* **2007**, *107*, 4797–4862.
13. Zabet-Khosousi, A.; Dhirani, A. A. Charge Transport in Nanoparticle Assemblies. *Chem. Rev.* **2008**, *108*, 4072–4124.
14. Zabet-Khosousi, A.; Trudeau, P. E.; Suganuma, Y.; Dhirani, A. A.; Statt, B. Metal to Insulator Transition in Films of Molecularly Linked Gold Nanoparticles. *Phys. Rev. Lett.* **2006**, *96*, 156403(1)−156403(4).
15. Muller, K. H.; Herrmann, J.; Raguse, B.; Baxter, G.; Reda, T. Percolation Model for Electron Conduction in Films of Metal Nanoparticles Linked by Organic Molecules. *Phys. Rev. B* **2002**, *66*, 075417(1)−075417(8).
16. Lin, V. S.-Y.; DiMagno, S. G.; Therien, M. J. Highly Conjugated, Acetylenyl Bridged Porphyrins—New Models for Light-Harvesting Antenna Systems. *Science* **1994**, *264*, 1105–1111.
17. Susumu, K.; Frail, P. R.; Angiolillo, P. J.; Therien, M. J. Conjugated Chromophore Arrays with Unusually Large Hole Polaron Delocalization Lengths. *J. Am. Chem. Soc.* **2006**, *128*, 8380–8381.
18. Duncan, T. V.; Susumu, K.; Sinks, L. E.; Therien, M. J. Exceptional Near-Infrared Fluorescence Quantum Yields and Excited-State Absorptivity of Highly Conjugated Porphyrin Arrays. *J. Am. Chem. Soc.* **2006**, *128*, 9000–9001.
19. Frail, P. R.; Susumu, K.; Huynh, M.; Fong, J.; Kikkawa, J. M.; Therien, M. J. Modulation of Dark Conductivity Over a 1×10^{-12} to 1×10^{-5} S/cm Range through Ancillary Group Modification in Amorphous Solids of Ethyne-Bridged (Porphinato)zinc(II) Oligomers. *Chem. Mater.* **2007**, *19*, 6062–6064.
20. Middleton, A. A.; Wingreen, N. S. Collective Transport in Arrays of Small Metallic Dots. *Phys. Rev. Lett.* **1993**, *71*, 3198–3201.
21. The $I-V$ characteristics of the dithiol−PZn_3 attached 32 nm AuNP sample has been modeled as $I \approx (V - V_T)^{\eta}$, where η was found to be 1.96, close to the predicted value for a 2D random metallic array.
22. Wang, G. N. R.; Wang, L. Y.; Qiang, R. D.; Wang, J. G.; Luo, J.; Zhong, C. J. Correlation Between Nanostructural Parameters and Conductivity Properties for Molecularly-Mediated Thin Film Assemblies of Gold Nanoparticles. *J. Mater. Chem.* **2007**, *17*, 457–462.
23. The $I-V$ characteristics were normalized with respect to dark current, using the following equation (red laser as an example): $(I_{Red} - I_{Dark})/\{$(no. of photons/sec/mm^2) $\times$ area of device$\}$. All current values corresponded to 1V.
24. Mangold, M. A.; Weiss, C.; Calame, M.; Holleitner, A. W. Surface Plasmon Enhanced Photoconductance of Gold Nanoparticle Arrays with Incorporated Alkane Linkers. *Appl. Phys. Lett.* **2009**, *94*, 161104(1)−161104(3).
25. Zangmeister, C. D.; Robey, S. W.; van Zee, R. D.; Yao, Y.; Tour, J. M. Fermi Level Alignment and Electronic Levels in "Molecular Wire" Self-Assembled Monolayers on Au. *J. Phys. Chem. B* **2004**, *108*, 16187–16193.
26. Sedghi, G.; Sawada, K.; Esdaile, L. J.; Hoffmann, M.; Anderson, H. L.; Bethell, D.; Haiss, W.; Higgins, S. J.; Nichols, R. J. Single Molecule Conductance of Porphyrin Wires with Ultralow Attenuation. *J. Am. Chem. Soc.* **2008**, *130*, 8582–8583.
27. Beebe, J. M.; Kim, B.; Gadzuk, J. W.; Frisbie, C. D.; Kushmerick, J. G. Transition from Direct Tunneling to Field Emission in Metal−Molecule−Metal Junctions. *Phys. Rev. Lett.* **2006**, *97*, 026801(1)−026801(4).
28. Susumu, K.; Therien, M. J. Decoupling Optical and Potentiometric Band Gaps in π-Conjugated Materials. *J. Am. Chem. Soc.* **2002**, *124*, 8550–8552.
29. Novotny, L. Nano-optics—Optical Antennas Tuned to Pitch. *Nature* **2008**, *455*, 887.
30. Muhlschlegel, P.; Eisler, H. J.; Martin, O. J. F.; Hecht, B.; Pohl, D. W. Resonant Optical Antennas. *Science* **2005**, *308*, 1607–1609.
31. Turkevich, J.; Stevenson, P. C.; Hillier, J. A Study of the Nucleation and Growth Processes in the Synthesis of Colloidal Gold. *Discuss. Faraday Soc.* **1951**, *11*, 55–75.
32. See Figure 4b, where a peak develops at ~450 nm after dithiol−PZn_3 attachment to the AuNP.
33. Li, X. L.; Xu, W. Q.; Wang, X.; Jia, H. Y.; Zhao, B.; Li, B. F.; Ozaki, Y. H. Ultraviolet−Visible and Surface-Enhanced Raman Scattering Spectroscopy Studies on Self-Assembled Films of Ruthenium Phthalocyanine on Organic Monolayer-Modified Silver Substrates. *Thin Solid Films* **2004**, *457*, 372–380.
34. Seth, J.; Palaniappan, V.; Johnson, T. E.; Prathapan, S.; Lindsey, J. S.; Bocian, D. F. Investigation of Electronic Communication in Multiporphyrin Light-Harvesting Arrays. *J. Am. Chem. Soc.* **1994**, *116*, 10578–10592.